OBSERVATION OF DELAYED PROTON RADIOACTIVITY

R. Barton, R. McPherson, R E. Bell, W. R. Frisken,
W. T. Link, and R. B. Moore

OBSERVATION OF DELAYED PROTON RADIOACTIVITY

R. Barton,* R. McPherson, R. E. Bell, W. R. Frisken,
W. T. Link, and R. B. Moore

Radiation Laboratory, McGill University, Montreal
Received August 14, 1963

ABSTRACT

The observation of delayed proton emission is reported. Bombardment of both aluminum and silicon with 97-Mev protons leads to the emission of delayed proton energy groups from 2 to 5 Mev. They follow the beta decay of Si^{25} ($T_{1/2}$ about 0.3 sec) to proton-unstable excited states of Al^{25}. Delayed protons were also observed following bombardment of Mg, Na, F, N, and O. The energy groups in the delayed proton spectra are explained by assuming that, in each case, a nuclide whose (Z, N) is of the form $(2k+2, 2k-1)$ is the parent nuclide, the decay chain being of the form:

$$(2k+2, 2k-1) \xrightarrow{\beta^+} (2k+1, 2k)^* \xrightarrow{p} (2k, 2k).$$
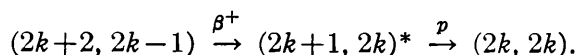
The observed delayed proton energies are those deduced by assuming that known levels of the intermediate nucleus emit the protons. Agreement of this kind, together with cross bombardment, threshold, and lifetime measurements, established the observation of the previously unreported Si^{25}. With less experimental detail, delayed protons have been assigned to the decay schemes of the previously unreported Mg^{21}, Ne^{17}, and O^{13}.

INTRODUCTION

Energy groups of delayed protons at 2 to 5 Mev have been observed following bombardment of Si, Al, Mg, Na, F, N, and O with 97-Mev protons in the new external beam of the McGill Synchrocyclotron. Only preliminary results are reported, which were obtained just before a planned shutdown of the cyclotron for construction purposes. This work will be resumed shortly. Brief reports of the central part of this work have been made by Barton and McPherson (1963a, b) and McPherson and Barton (1963). This paper is adapted from the Ph.D. thesis of Barton (1963).

In general, there seem to be three mechanisms through which proton emission that is delayed by a measurable time could occur. (In this experiment all recorded events were delayed by at least 200 μsec.) The three phenomena will be referred to as: (1) self-delayed proton emission, (2) self-delayed double proton emission, and (3) beta-delayed proton emission. Goldansky (1960, 1961) has discussed these possibilities in some detail. Item (1), self-delayed proton emission, refers to the emission of a low-energy proton delayed by a measurable time owing to the presence of the nuclear Coulomb barrier. (In this language, ordinary α decay would be called self-delayed α emission.) Simple barrier penetration calculations lead to the conclusion that for Z from 10 to 15, energies about 100 kev may be low enough. Item (2), self-delayed double proton emission, was originally proposed by Goldansky. He predicts that near the edge of proton instability, the binding energy of an even-Z nuclide may be smaller than the energy by which the odd-Z nuclide one proton lighter is

*Present address: Physics Department, Loyola College, Montreal.

unbound. Thus the heavier nuclide is stable against one-proton decay but unstable against the emission of two protons. Whether one assumes that two individual protons must both penetrate the Coulomb barrier almost simultaneously or that a pair of protons (intranuclear diproton) with its doubled charge and mass must penetrate the Coulomb barrier, simple calculations lead to identical measurable lifetimes. Item (3), beta-delayed proton emission, refers to the branching of the beta decay of a nuclide with large Q_{β^+} to a proton-unstable excited state of the daughter nuclide. In this case the protons would exhibit the lifetime of the beta decay. Goldansky lists nuclides from which each of the above phenomena are to be expected, along with predictions of lifetimes and proton energies.

In this work we have observed beta-delayed proton emission. This is completely analogous to beta-delayed neutron emission, which was first observed by Roberts et al. (1939) and Booth et al. (1939). Pappas and Rudstam (1960) discuss the systematics of delayed neutron emission.

Of the three possible types of delayed proton emitters, one can expect, with a 97-Mev proton beam, to produce beta-delayed proton emitters with considerable probability. On the other hand, the self-delayed p and $2p$ emitters are at the edge of proton instability, sufficiently far from the stable nuclides so that with such a beam one does not expect to produce them with observable intensity.

EXPERIMENTAL ARRANGEMENTS

External Beam

The proton beam used in these bombardments was extracted from the maximum-energy orbit of the McGill Synchrocyclotron by the d-c. magnetic regenerative technique (Moore 1962; Le Couteur 1955). The design of this extraction system and the character of the beam after transport into the new Radiation Laboratory beam hall will be published later. In Fig. 1 the section in the median plane of the cyclotron shows the configuration of the regenerator and extraction channel, together with the simple system used to transport the external proton beam to the temporary experimental station. The self-excited quadrupole sections of the extraction channel were carefully adjusted to render the proton beam optimally parallel as it left the region of strong fringing field. Thus even the weak focusing of the steering magnet was enough to give an average beam intensity of 3×10^{10} protons/second through an area of 2 cm^2 at the target station, 10 m from the cyclotron. The geometrical spread of the beam is smaller than 5 cm-milliradians both vertically and horizontally.

The mean proton energy, determined from the extrapolated range in aluminum, is 97.0 ± 0.3 Mev, and preliminary measurements of the energy spread indicate that the FWHM is considerably less than 1 Mev.

Apparatus

Figure 2 gives a representation of the main features of the target chamber. It was evacuated to avoid counting radiations from air and to allow the counting of protons of as low an energy as possible; its vacuum was made separate

TARGET CHAMBER

CYCLOTRON VACUUM CHAMBER

LAST STABLE ORBIT

CONCRETE SHIELDING

DEFLECTED ORBIT

DEFLECTION CHANNEL

39° BENDING MAGNET

REGENERATOR
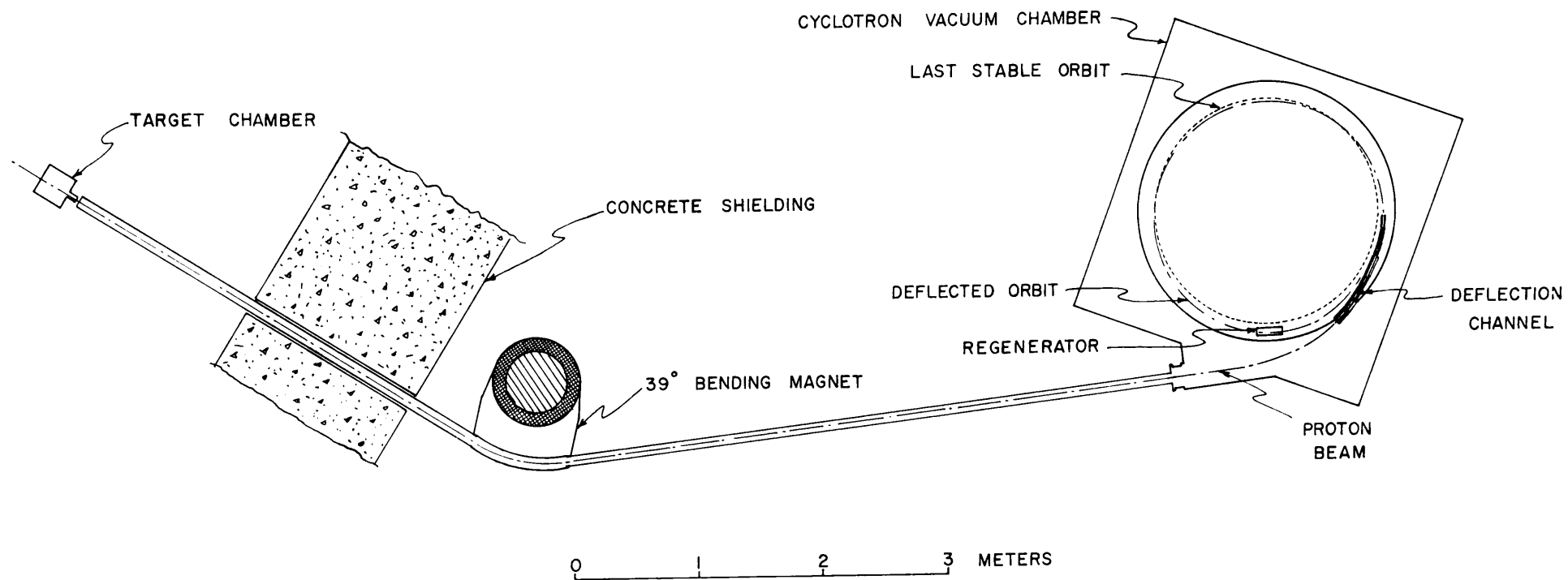
PROTON BEAM

0   1   2   3   METERS

FIG. 1. Section in the median plane of the cyclotron, including extraction system, beam transport system, shielding, and position of target chamber.
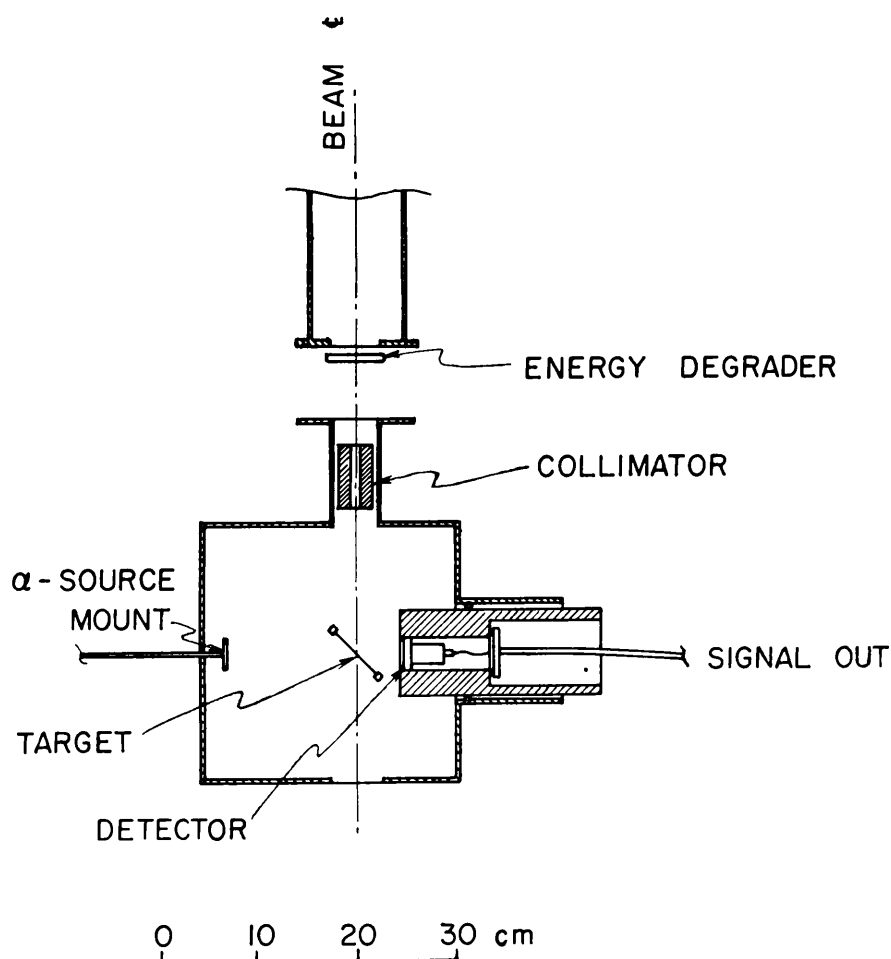
FIG. 2. Schematic representation of the target chamber. The indicated detector is a silicon-junction particle detector. The energy degrader and collimator were used only when obtaining activation curves.

from that of the beam pipe for convenience. The end windows of the chamber were not visible to the counter so that no direct radiations from them were counted. For the purpose of obtaining activation curves, protons of energy lower than 97 Mev were obtained by placing aluminum absorbers of appropriate thickness against the end of the beam pipe. A collimator was then placed as indicated in Fig. 2. In order to calibrate the system for energy response a Po^{210} α source was mounted on the end of the rod that goes through the chamber wall directly opposite the counter. The source was removed whenever any counting was done.

The counter, a silicon junction particle detector, was protected from the fringe of the beam by the thick-walled aluminum cylinder in which it was mounted. A short piece of coaxial cable (13 pf/ft) connected the detector to the input of a Tennelec low-noise charge-sensitive amplifier. The face of the counter was 1 in. from the axis of the beam. At this distance the effects of scattered protons from each beam burst were such that the electronic system recovered sufficiently for counting to be resumed after 200 μsec. In order to eliminate delayed-α background and to obtain range–energy curves for the observed energy groups, thin aluminum foils were placed flat on the end of the counter-protecting cylinder.

The beam current was monitored via a 7-in. Faraday cup placed a few feet downstream from the exit port of the chamber.

Figure 3 gives a schematic representation of the cyclotron and counting cycles and of the electronic system. The purpose of this apparatus was to store pulse-height information during a selected portion of the interval between beam bursts. The counting interval started 200 μsec after each beam
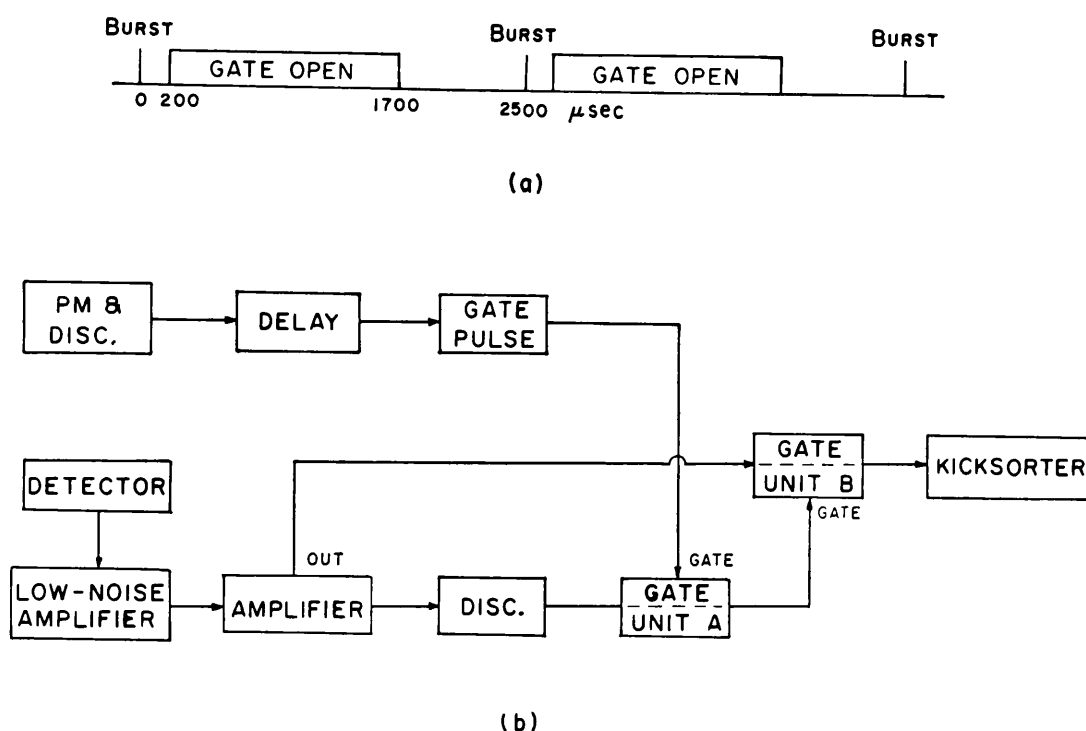

FIG. 3. (a) Schematic representation of the cyclotron and counting cycles. (b) Block diagram of electronics.

burst and extended to 1700 μsec after each burst; if it were any longer it would allow the registering of spurious pulses picked up from the firing-on of the oscillator for the next cyclotron burst. Thus every recorded count was delayed by at least 200 μsec.

In order to calibrate the system for energy response, i.e., to find the relationship between kicksorter channel and energy absorbed in the detector, the following procedure was used. First a pulse generator giving a long, fast-rising pulse was connected to the input of the low-noise amplifier via a 1-pf capacitor. The height of this pulse, and therefore the charge deposited at the amplifier, was precisely controllable by a potentiometer. Using a series of well-known α lines a strict proportionality between α energy and potentiometer setting was established. Therefore after the potentiometer settings were interpreted as energy, the dial being recalibrated from time to time using the Po^{210} α line.

MEASUREMENTS, RESULTS, AND DISCUSSION

In this section the observation of delayed protons following the bombardment of aluminum and the reasons for assigning these to the decay of Si^{25} will be described in detail. Further, the observation of heavy charged-particle

energy groups from various other targets will be reported and an explanation of them that is completely analogous to the Si^{25} explanation for the aluminum target will be given.

Delayed Protons from Aluminum

Because of very intense background up to about 2.5 Mev due to beta particles and gamma rays, it was not possible to detect any heavy charged particles below this energy. In order to investigate as great an energy range as possible, the RCA F-3-25-2.0 counter, whose rated bias is 25 v, was operated regularly at 100 v. This seemed to have no effect on the resolution of the system but it did create problems of long-term stability. After some energy groups were found, the detector resistivity was found by plotting the apparent energy of the end of the spectrum against detector bias. The result was a resistivity between 3000 and 5000 ohm-cm. Consequently, with 100-v bias, the thickness of the depletion layer was equal to the range of a proton with energy between 4.5 and 5.0 Mev. Thus it was found possible to investigate the energy range from about 2.5 to about 4.5 Mev without distortion or displacement of the peaks. Mainly because of the background conditions, the observed width of monoenergetic peaks was rather large, about 250 kev.

Without any target in the counting chamber it was found that during a run of typical length about 20 counts would be distributed over the energy range under investigation. This is completely negligible.

An aluminum foil 2.15 mg/cm² thick was placed in the target holder (Fig. 2) so that it was in a vertical plane that made an angle of 23° with the direction of the beam. Thus it was thicker along the direction of the beam than along the line joining it to the counter. The distance from the counter to the beam axis was 2.46 cm, and the counter's area was 200 mm² so that the geometrical efficiency was about 2.5%. As was previously stated, the delayed gate pulse allowed counts to be recorded during the 1500-μsec interval from 200 to 1700 μsec after each burst. Since the cyclotron period was held very close to 2500 μsec, the counting period occupied 60% of the time; if the lifetimes of the radiations were long compared to 2500 μsec, as they seemed to be, this effectively made the counting efficiency 60% of the geometrical efficiency. With this information, together with the target thickness and beam current, cross sections for the production of delayed protons were estimated.

The delayed spectra following the bombardment of aluminum must be classified into those recorded with a thin or no absorber foil and those recorded with thicker absorbers. With a 4.3 mg/cm² or thicker Al foil as absorber the proton peaks stand out quite sharply. With a 2.15-mg/cm² absorber or with no absorber, the proton spectrum is at least partly buried under a more intense continuum. This continuum is such that 4.3 mg/cm² of absorber will degrade its uppermost energy from at least 5 Mev to at most 2 Mev. This continuum, is therefore, made up of alpha particles because at 5-Mev energy only an alpha line would be spread into a continuum by a 2.15-mg/cm²-thick source and still get through a 2.15-mg/cm²-thick absorber. It is highly probable that the major source of these alphas is Na^{20}, produced in the reaction $Al^{27}(p, p\alpha 3n)Na^{20}$. This known nuclide has a beta half-life of 0.3 sec and leads to excited states of Ne^{20} that emit alphas of appropriate energy.

With the thicker absorbers in place a spectrum consisting of sharp lines is observed. (See Figs. 4 and 5 for examples of such spectra.) These lines unquestionably occur only when the target is in place, but the question remains whether they are delayed radiations from the target or from the counter itself, which is made of silicon. The latter could be the case if, for example,

DELAYED SPECTRUM FROM ALUMINUM TARGET

beam	97 Mev protons
target	2·15 mg/cm² Al
absorber	8·60 mg/cm² Al
running time	1·3 hr
counting cycle	200 to 1700 μsec after burst
cyclotron period	2500 μsec

SPECTRUM WITH
BACKGROUND
SUBTRACTED

p_2Al

p_3Al p_1Al

ORIGINAL SPECTRUM

Estimated
background
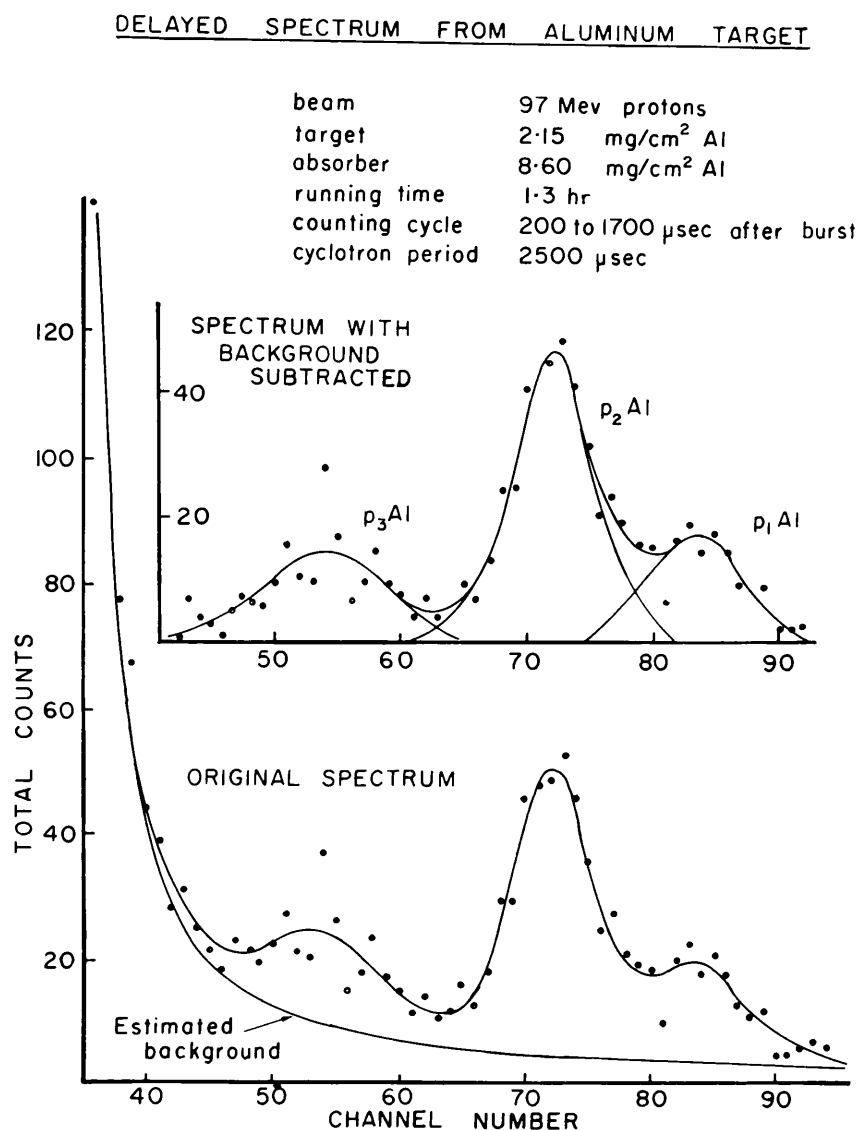
TOTAL COUNTS

CHANNEL NUMBER

FIG. 4. Spectrum of delayed heavy charged particles from aluminum target. The estimated background was drawn in by hand and subtracted from the original spectrum.

the cross section for production were very much larger in silicon than in aluminum, and protons scattered into the counter by the target initiated the reaction. However, the counted particles must come from the target because, as will be seen later, the qualitative appearance of the spectrum changes when different materials are used in target foils of roughly the same thickness.

Thus energy groups of heavy charged particles that are emitted from the target after a delay of at least 200 μsec have been observed. Figure 6 demonstrates that these lines are due to protons. These graphs were obtained from absorption data: various thicknesses of Al absorber foil were placed over the end of the counter shield and the energy of each peak was determined. The observed energies of the peaks p_2Al and p_3Al, as they are labeled in Fig. 4, are plotted against absorber foil thickness. Residual energy curves are plotted
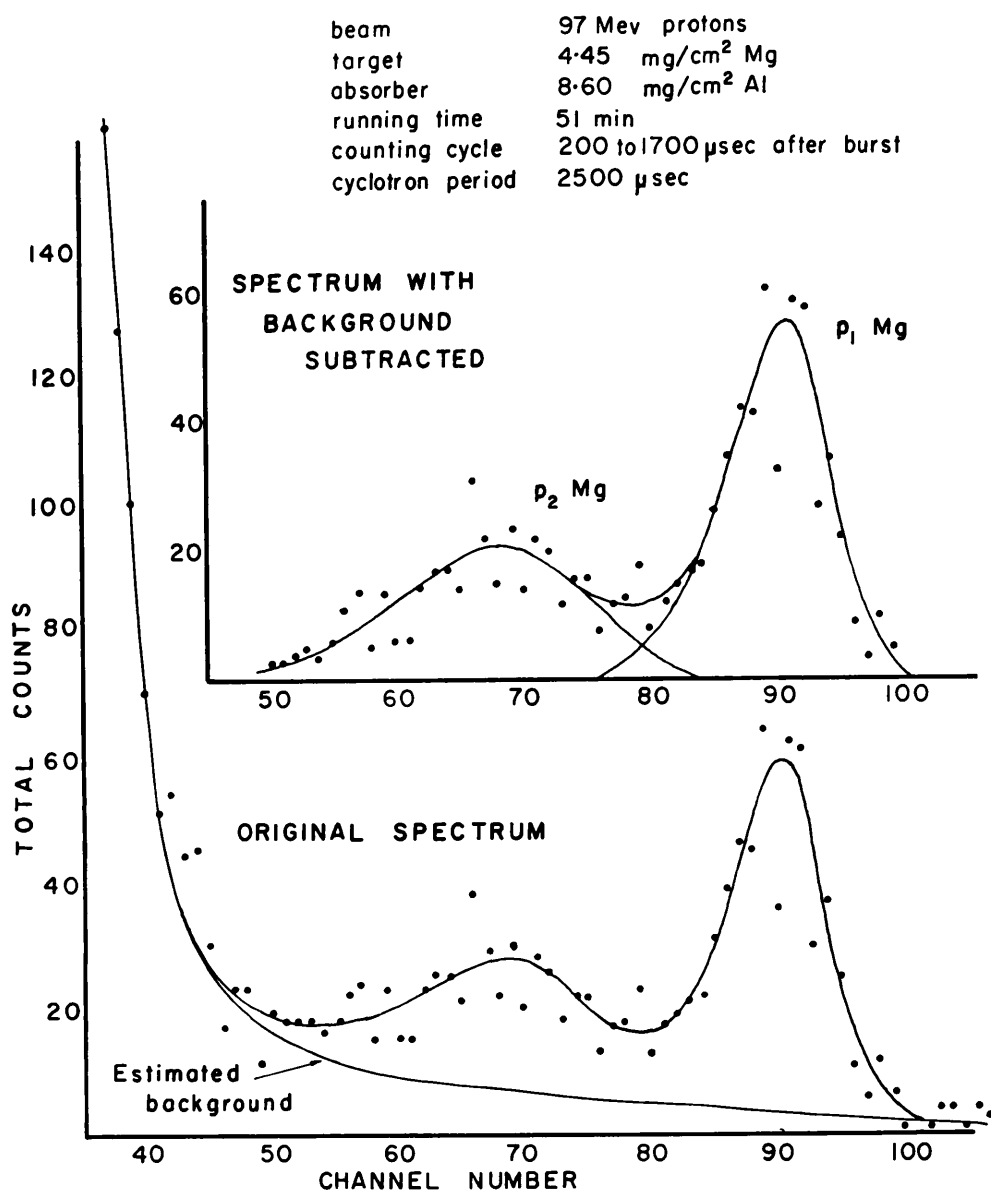
FIG. 5.   Spectrum of delayed heavy charged particles from magnesium target.

for both protons and deuterons. Clearly the observed points lie on curves that fall much too slowly for deuterons or any more heavily ionizing particle, while they are well fitted by proton curves. Only two points were obtained for p_1Al because the highest-energy point was too close to the range of the detector to be reliable: no data for this peak are plotted. The data are consistent with p_1Al being due to protons.

It remains to show that these delayed protons are from the bombardment of aluminum and not from some impurity, e.g., the oxygen in the oxide coating on the aluminum foil. This is most convincingly shown by the fact that no other target yielded a very much higher counting rate, including a target of oxygen-containing air.

Si^{25}, a Source of Beta-Delayed Protons

Although only p_2Al and p_3Al have been shown conclusively to be protons, it will be assumed that all the peaks in each of the spectra to be described
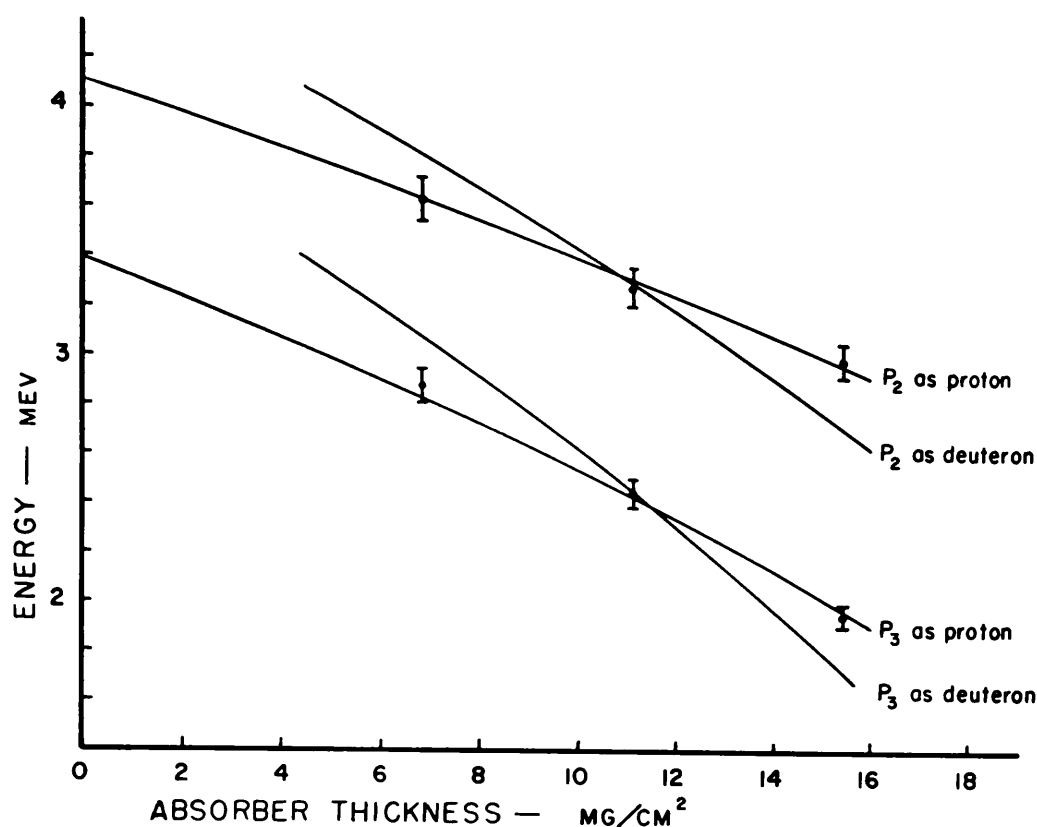
FIG. 6. Residual energy curves showing that the observed peaks are due to protons. The curves are for protons and deuterons of the indicated initial energies. The points represent experimental data.

are due to protons. This is a proper assumption for two reasons. First, as will be seen, all the peaks observed can be accounted for in the same fashion from this assumption. Second, it is hard to see how any other particle can possibly be observed: no neutron-containing delayed particles, except alphas, can be emitted by neutron-deficient light nuclides because the neutron binding energies are as large as the Q values for beta decay; the possibility of observing alphas is eliminated because any alpha that penetrated the 9 mg/cm² of absorber that was normally over the counter would have to be emitted with at least 12 Mev energy, which again is as large as the Q values for beta decay. Therefore, since some of the peaks have been shown to be protons, since each of the others can be accounted for by assuming that it is due to a proton, and since it is highly doubtful that any other type of delayed radiation could be observed, it will be assumed that all the peaks are due to protons.

Various targets were bombarded and the delayed spectrum recorded in each case. All of these spectra are very similar to that for Al. In all cases, statistics were very poor with consequent large uncertainties in energy and cross section. Table I gives the measured properties of all the intense lines observed. The energy values have been corrected for target, absorber, and counter window thicknesses. Table I also gives cross sections for the production of the proton peaks; usually these turn out to be a few microbarns, but less than one microbarn for an air target.

Having established that delayed protons were emitted following the bombardment of aluminum, an attempt was made to find what type of delayed

TABLE I

Target	Energy of line, Mev	Designation	Molecular cross section, μb	Threshold energy, Mev	Half-life, sec
SiO_2	4.65 ± 0.1	p_1Si	4.6 ± 0.3	$\left.\begin{array}{c}\\\\\end{array}\right\}\sim50$	$0.3^{+0.2}_{-0.1}$
	4.17 ± 0.1	p_2Si	16 ± 1		$0.3^{+0.2}_{-0.1}$
	3.39 ± 0.1	p_3Si	6.2 ± 0.4		$0.3^{+0.4}_{-0.1}$
Al	4.55 ± 0.1	p_1Al	1.4 ± 0.1		
	4.10 ± 0.1	p_2Al	3.3 ± 0.2		
	3.39 ± 0.2	p_3Al	1.6 ± 0.1		
Mg	4.71 ± 0.1	p_1Mg	3.0 ± 0.2		
	4.02 ± 0.1	p_2Mg	2.0 ± 0.1		
LiF	4.68 ± 0.1	p_1F	7.0 ± 0.4		
	$3.6\ \pm0.1$	p_2F	~1		
NaF	4.5 (broad)	p_1NaF	10 ± 1		
	3.7 (broad)	p_2NaF	4.3 ± 0.2		
$N_{4.5}O$ (air)	4.50 ± 0.1	p_1Air	0.14 ± 0.02		
	3.97 ± 0.1	p_2Air	0.07 ± 0.02		

proton emission was taking place and what the parent nuclides responsible for the delays were. Accordingly, targets of magnesium and silica (SiO_2) were bombarded. The cross sections for oxygen (air target) are so small compared to those for silica (see Table I) that one may assume that all the silica activities are from the bombardment of silicon. Now, p_1Al, p_2Al, and p_3Al each has an analogous peak of the same energy within errors in the spectrum from the silicon target; furthermore, the cross sections in the case of silicon have about the same relative values as those for the case of the aluminum target. It is, therefore, highly probable that these two spectra are of the same set of radiations from the same parent nuclide produced in different ways.

In the spectrum from the magnesium target, Fig. 5, p_3 is entirely missing and the relative intensities of p_1 and p_2 are reversed. Clearly, then, the lines from aluminum and silicon are being produced only weakly, if at all, in the bombardment of magnesium. Recalling that in a proton cyclotron the projectile has one unit of charge, we may assume that corresponding lines from the aluminum and silicon targets have common parent nuclides that are isotopes of silicon; it is then impossible to produce these lines in a bombardment of magnesium.

The activation curves shown in Fig. 7 were obtained by bombarding silicon at the various energies indicated on the graphs. Degrading and collimating of the beam was done as previously explained. The semilogarithmic plot in Fig. 7 shows that the three proton lines have the same parent nuclide, for the curves are vertically separated by constant distances and hence are in constant ratios to one another. The linear plot shows that the three lines have the same apparent threshold at about 50 Mev. The threshold for the reaction $Si^{28}(p, p2n)Si^{26}$ can be calculated from known β-decay Q values (Ajzenberg-Selove and Lauritsen 1959) and is 31.6 Mev (lab.). Using, in conjunction with this value, estimates of neutron separation energies (Seeger 1961), one finds the threshold for $Si^{28}(p, p3n)Si^{25}$ to be 49.8 Mev and for $Si^{28}(p, p4n)Si^{24}$ to
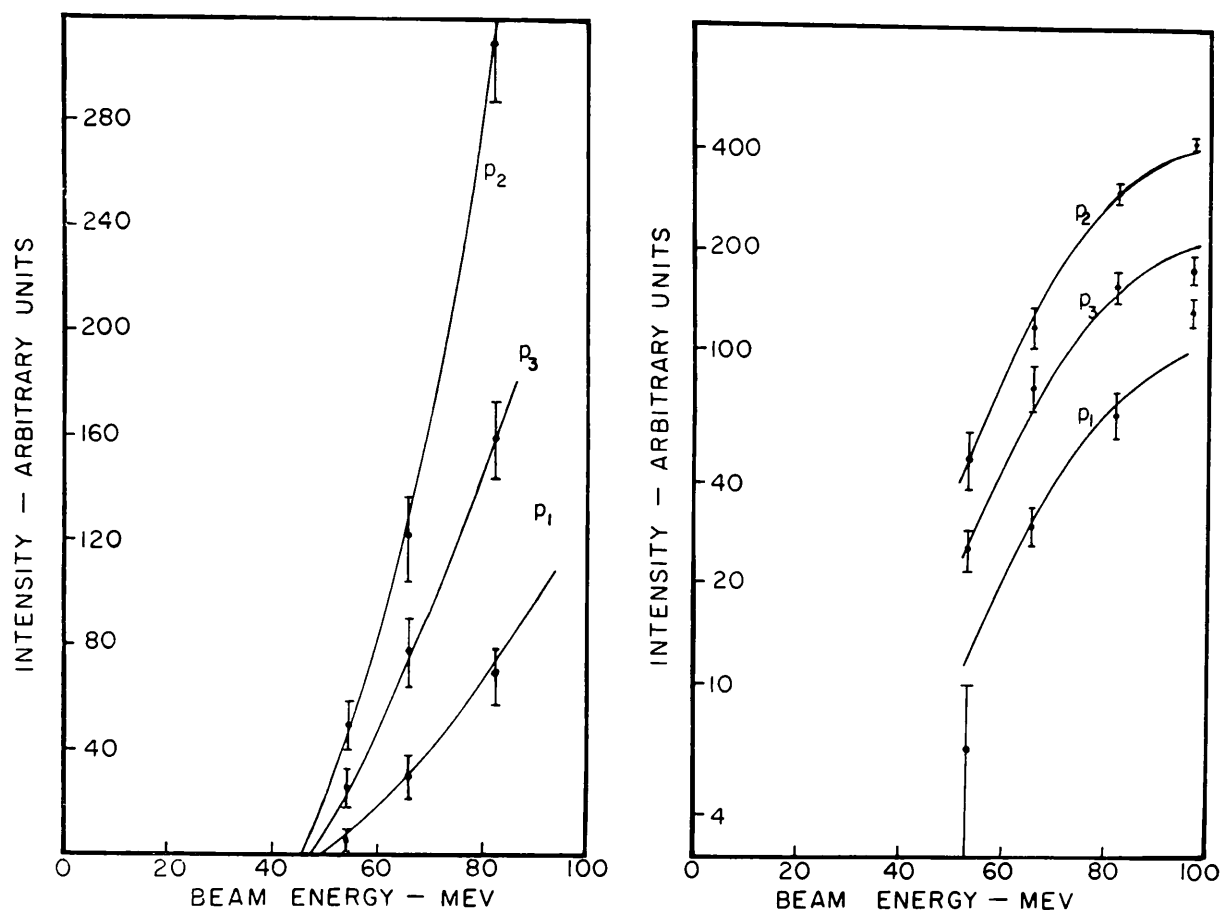
FIG. 7. Activation curves for the three peaks of the spectrum obtained from a Si target. The semilogarithmic plot on the right exhibits the constant ratios between the three energy groups. The linear plot on the left exhibits the common threshold energy at about 50 Mev.

be 64.7 Mev. Because of the shape of the curves near threshold and because of the close agreement between the measured thresholds and that calculated for producing Si^{25}, we conclude that Si^{25} is the parent nuclide for all three proton lines. This conclusion is reinforced by noting that a less complete activation curve for production of the same protons from an aluminum target showed a threshold below 40 Mev, consistent with $Al^{27}(p, 3n)Si^{25}$, which has an estimated threshold of 37.8 Mev.

Further, the lifetimes of the three lines from the Si target were measured. This was done by gating the cyclotron on for 1 second and off for 1 second. During the off period the pulse-height spectrum was accumulated for consecutive $\frac{1}{4}$-second periods in three of the quarters of the kicksorter's memory, producing a three-point decay curve of the whole spectrum. Figure 8 shows the results obtained for each peak. The lines were drawn parallel with a slope corresponding to a $T_{1/2}$ of 0.3 sec. This fit is evidently consistent with the data. The equality of these lifetimes is further confirmation that the three peaks are products of the decay of a single nuclide.

The nuclide Si^{25} has 14 protons and 11 neutrons. The nuclides Mg^{25} and Al^{25} are known to be deformed with $\delta = 0.3$ approximately (Mottelson and Nilsson 1959). Assuming that Si^{25} is similarly deformed, the Nilsson diagram predicts $3/2^+$ for its ground state. On the other hand the ground state of its mirror nucleus, Na^{25}, has been assigned as $5/2^+$ (Endt and van der Leun 1962). One
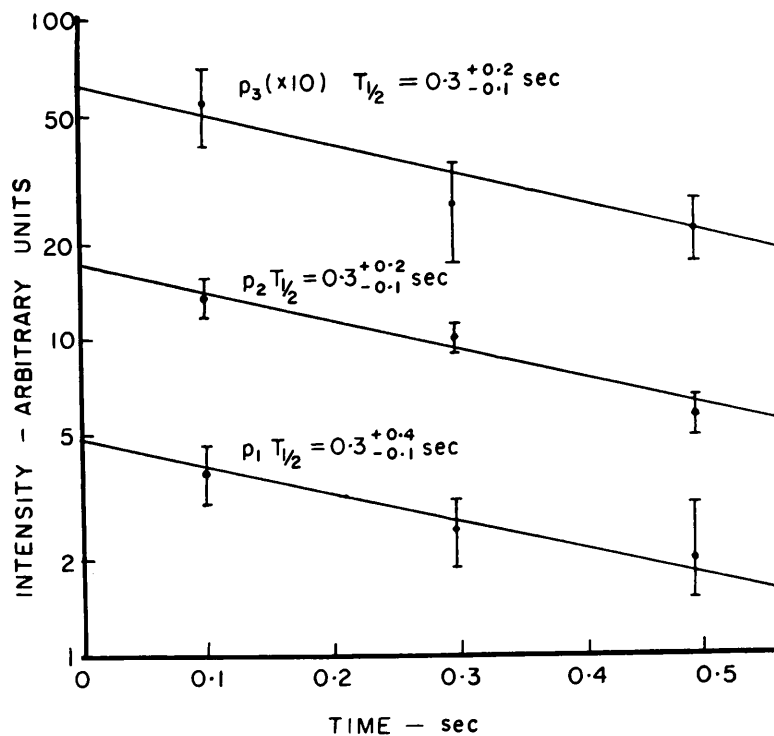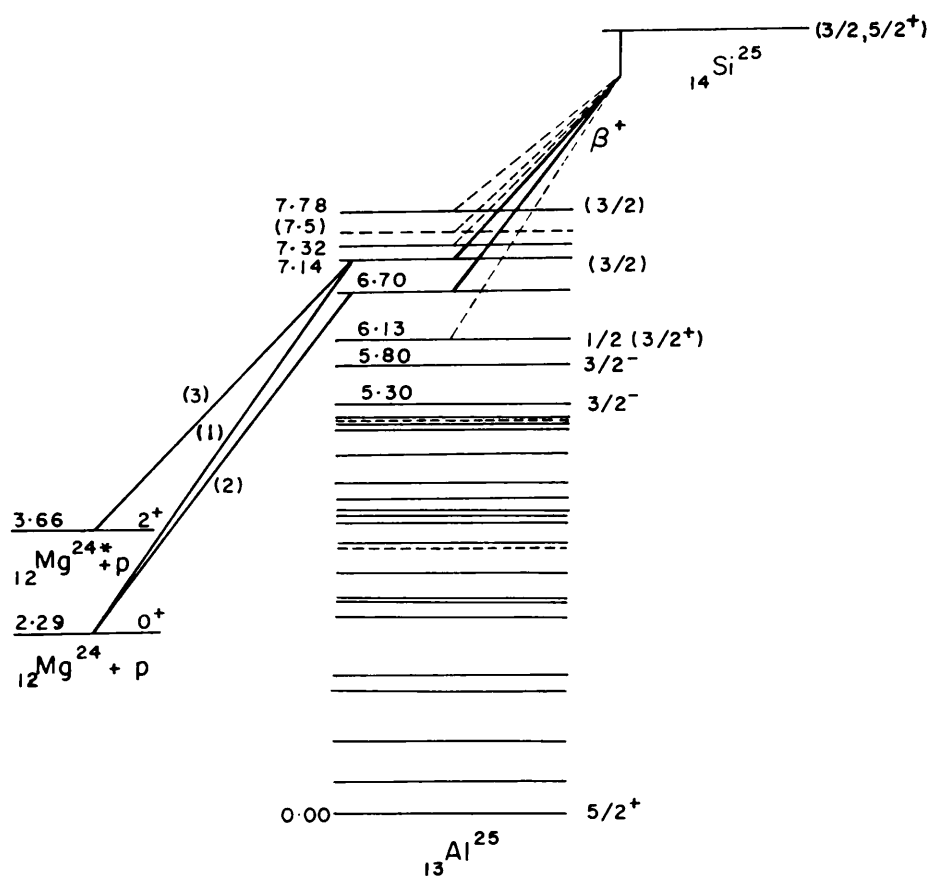
FIG. 8. Decay curves of the three peaks from a silicon target, exhibiting the common half-life of about 0.3 sec. This, therefore, is the half-life of Si²⁵.

may, therefore, assume that the spin-parity of the Si²⁵ ground state is either $3/2^+$ or $5/2^+$. Hence Si²⁵ decays by an allowed beta transition to the ground state of Al²⁵ and the lifetime can be estimated accordingly. Using Seeger (1961) to obtain an estimate of 10.3 Mev for the Q value, and assuming a $\log ft$ of about 5, one obtains a half-life of the order of 1 sec, in agreement with this experiment. Since the lifetime of a self-delayed 3-Mev proton from Si cannot possibly be as large as 0.3 sec, since Si²⁵ is certainly stable against particle emission, and since the observed lifetime of Si²⁵ agrees with that calculated from the theory of beta decay, we conclude that the observed proton lines are beta-delayed protons emitted from excited states of Al²⁵ following the beta decay of Si²⁵.

Figure 9 shows the proposed decay scheme. The peak p_2Si, the most intense one, is attributed to the decay of the 6.70-Mev state of Al²⁵ to the ground state of Mg²⁴. This transition is labeled (2). A proton line at 2.92 Mev due to the decay of this level to the first excited state of Mg²⁴ should also occur, but after being degraded in energy by 10 mg/cm² of material it would have been hidden under the high background just below 2 Mev and hence not observed. The peaks p_1Si and p_3Si are attributed to the decay of the 7.14-Mev level of Al²⁵ to the 0⁺ ground state and the 2⁺ first excited state of Mg²⁴. The observed intensities of p_1Si and p_3Si are about equal, consistent with the relative energies and spin-changes of these two branches. The intensity of p_2 is somewhat greater than the sum of those of p_1 and p_3, consistent with the slightly greater transition energy for beta decay to the 6.70-Mev level of Al²⁵. Finally, since no level of Al²⁵ in the energy range of interest is known to have a spin and parity appropriate to an allowed beta transition from Si²⁵, this proposed decay scheme does not ignore any expected lines. Thus the proton spectrum from the Al and Si targets is accounted for.

proposed transition	proton energy (c.m.)	(lab.)	observed energy	target
(3)	3·48	3·34	3·39 3·39	Si Al
(1)	4·85	4·66	4·65 4·65	Si Al
(2)	4·41	4·23	4·17 4·10	Si Al

FIG. 9. Proposed decay scheme of Si[25] and a comparison of predicted and observed energies. The dashed lines indicate transitions not ruled out by energy or known spin-parity considerations but not leading to observed proton lines.

In summary, it is concluded that all the observed peaks are due to delayed protons and that the spectra from Al and Si targets are due to the same radiations. It is concluded from activation and lifetime evidence that these protons are beta-delayed protons emitted from excited states of Al[25] following the beta decay of Si[25]. A decay scheme is proposed that accounts for the observed spectrum and indicates that the 6.70- and 7.14-Mev levels of Al[25] have positive parity.

Intense Lines Due to (2k+2, 2k−1) Nuclides

The nuclide Si[25] is in a very favorable position to be parent to delayed protons for two reasons. First, its (Z, N) is of the form $(2k+2, 2k−1)$ so that it is parent to the following chain of decays:

$$(2k+2, 2k−1) \xrightarrow{\beta^+} (2k+1, 2k)^* \xrightarrow{p} (2k, 2k).$$

It is well known that nuclei of the form $(2k+1, 2k)$, one proton larger than an "alpha-particle nucleus" of the form $(2k, 2k)$, have exceptionally low proton separation energies. Second, each of the $(2k+2, 2k-1)$ nuclides up to a Z of 20 inclusive is the heaviest isotope of its element that has a large Q value for beta decay. This combination of low separation energy and large Q value means that β transitions to levels that can yield protons in the energy range of interest have a relatively large transition energy. No neighboring nuclide possesses this combination to the same degree and has a favorable production cross section.

Thus one would expect the spectrum from a Si target to be dominated by protons from the decay of Si^{25} and the spectrum from a Mg target to be dominated by protons from Mg^{21} decay, the next lighter $(2k+2, 2k-1)$ nuclide. From an Al target one would perhaps expect Si^{25} and Mg^{21} lines. However, identifying Mg^{21} lines with the spectrum from a Mg target, we have seen that there seems to be little, if any, contribution by this nuclide to the spectrum from an Al target. So the reaction $Al^{27}(p, 3n)Si^{25}$ seems more probable than the combined reactions $Al^{27}(p, 2p5n)Mg^{21}$ and $Al^{27}(p, \alpha3n)Mg^{21}$. This is perhaps fairly reasonable. One suspects, however, that with better resolution and statistics some contribution from Mg^{21} due to the $(p, \alpha3n)$ reaction might be observable.

In summary, one expects lines from the decay of $(2k+2, 2k-1)$ nuclides to dominate the delayed proton spectra from targets of all elements up to and including calcium (Z of 20). This is because these nuclides are in a much more favorable position, energetically, to decay to proton-emitting states than are their neighboring nuclides. Furthermore, $(p, 3n)$ reactions seem to be more probable, in these light elements, than $(p, \alpha3n)$ and $(p, 2p5n)$ reactions combined. This leads to the proton spectrum from targets of both element $(2k+1)$ and element $(2k+2)$ being dominated by protons in the decay of nuclide $(2k+2, 2k-1)$. In accordance with this last hypothesis, the decay of Mg^{21} should account for the spectra obtained from Mg and Na targets, the decay of Ne^{17} for the spectrum from a F target, and the decay of O^{13} for the spectrum from O and N targets.

Figures 10, 11, and 12 contain all the information relevant to the verification of this prediction. They were constructed in the following way. In the known level scheme of the intermediate nuclide, i.e., of the daughter of the beta decay, the parent nuclide is assigned a ground-state spin and parity as given by the shell model. All possible beta transitions which, on the basis of known level properties and the assumed ground-state properties of the parent, are thought to involve forbidden transitions are ignored. All other possible transitions that can lead to protons in the observed energy range are shown. Those shown by a dashed line do not lead to an observed proton line. The important points are, first, that all the observed proton energies are accounted for in this way, and second, that all transitions thought to be allowed, on the basis of known level properties, lead to an observed proton energy.

In the case of Mg^{21}, the indicated transitions in Fig. 10 clearly account for the observed spectrum from the Mg target. It will be explained shortly how
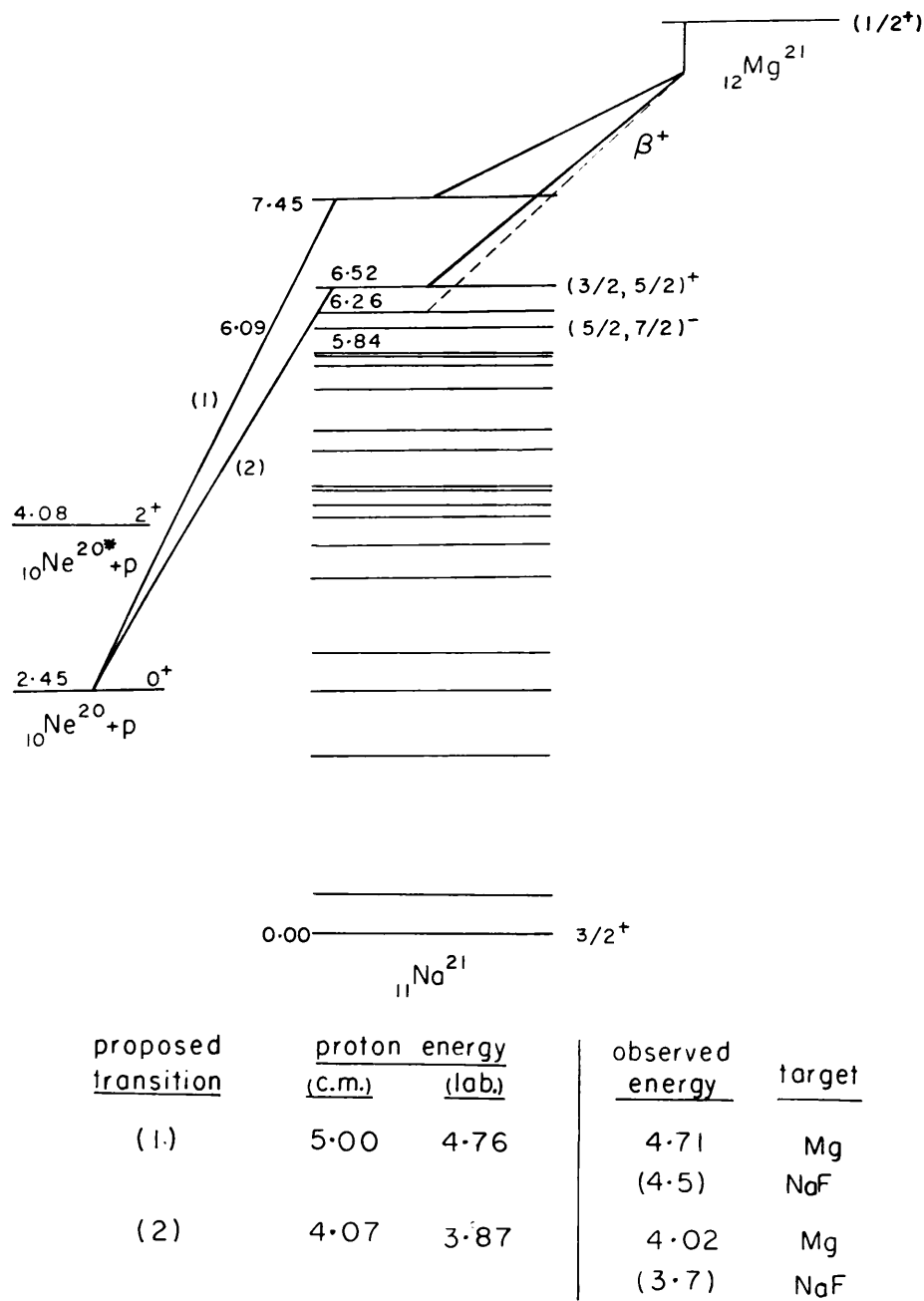
proposed transition	proton energy (c.m.)	proton energy (lab.)	observed energy	target
(1.)	5·00	4·76	4·71	Mg
			(4·5)	NaF
(2)	4·07	3·87	4·02	Mg
			(3·7)	NaF

FIG. 10. Proposed decay scheme from Mg[21] and a comparison of predicted and observed energies. The dashed lines indicate transitions not ruled out by energy or known spin-parity considerations but not leading to observed proton lines.

the spectrum resulting from bombardment of Na in the NaF target was deduced. It is the same as the Mg target spectrum and hence is also accounted for.

In the case of Ne[17] (Fig. 11) there is an initial ambiguity when trying to explain the spectrum from the LiF target. It is uncertain whether the 5.45- or 5.66-Mev level is responsible for the 4.68-Mev observed line. However, the lines in the spectrum from the NaF target were about 375 kev wide and the system resolution for single proton lines is 250 kev. If the spectrum from the Na part of the target is the same as that from Mg, there is a line at 3.87 Mev from the Na target and a line at 3.6 Mev from the F target. This accidental doublet accounts for the broad lower-energy peak from the NaF target. Trying to explain the other broad peak in the same way, one must discard the 5.60-Mev
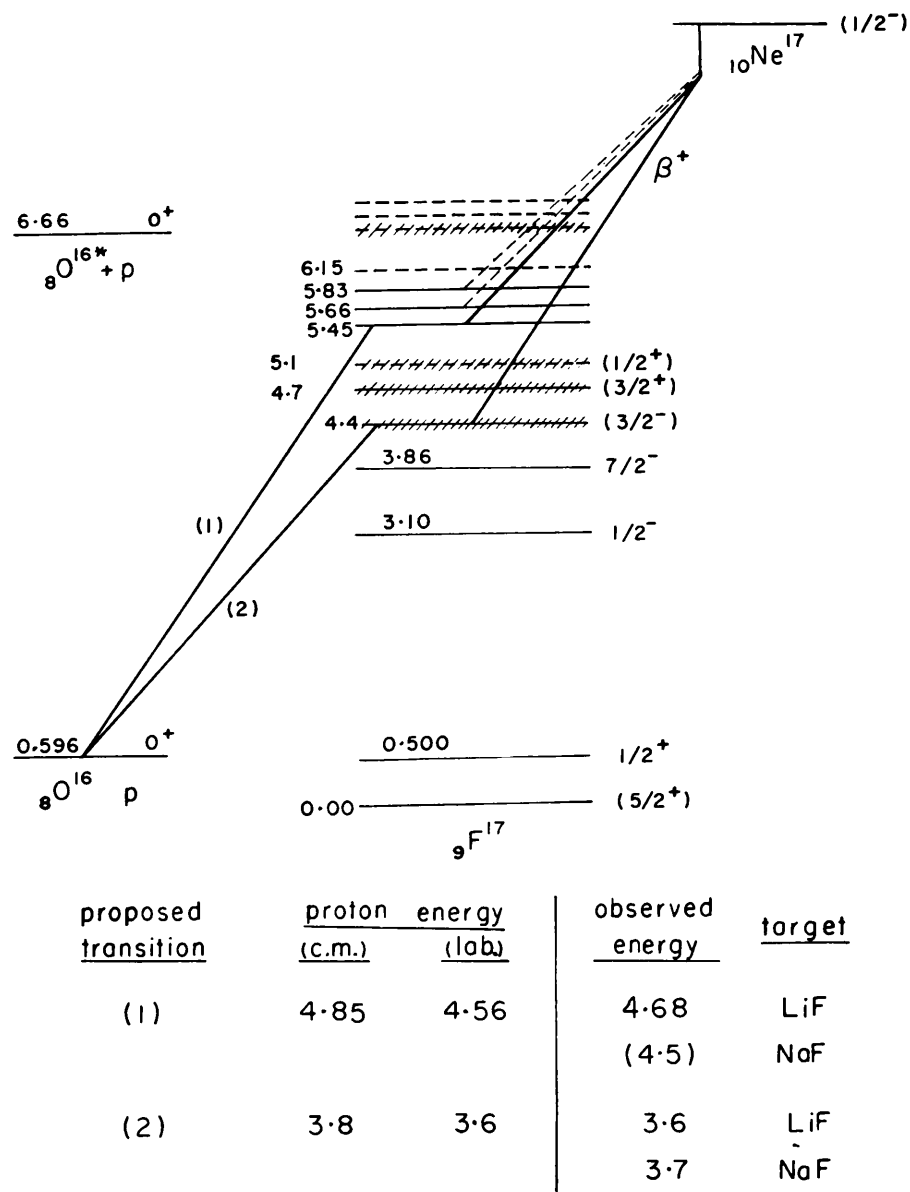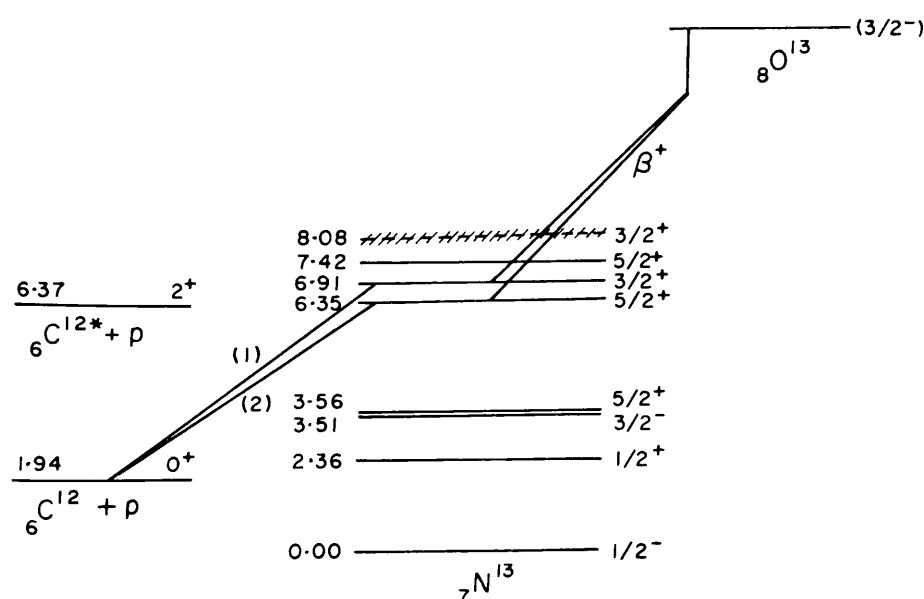
FIG. 11. Proposed decay scheme from Ne¹⁷ and a comparison of predicted and observed energies. The dashed lines indicate transitions not ruled out by energy or known spin-parity considerations but not leading to observed proton lines.

level in Ne^{17} because it leads to protons of the same energy as the higher-energy line from the Na target. Therefore, by explaining the spectrum from the LiF target and the anomalously broad peaks of the NaF target together, one gets an unambiguous picture of the Ne^{17} decay and confirms that Mg and Na targets both lead to Mg^{21} decay.

The case of O^{13} (Fig. 12) is slightly different from the other two cases. To the levels of the beta-decay daughter in the energy range of interest there can be no allowed beta transitions. However, there are possibilities for first-forbidden transitions, and these do in fact account for the observed spectrum from the air target, which contains the elements N and O. The forbiddenness of these transitions is consistent with the low cross sections observed since they compete with allowed transitions to low-lying levels.

The objection might be raised that these observed lines could come from the decay of nuclides neighboring those mentioned. Perhaps some or all lines from the F target have F^{15} for their source. Since sufficient information on the

$(3/2^-)$ — $_8O^{13}$

β^+

8·08	$3/2^+$
7·42	$5/2^+$
6·91	$3/2^+$
6·35	$5/2^+$

6·37 2^+
$_6C^{12*} + p$

(1)

(2) 3·56 — $5/2^+$
3·51 — $3/2^-$

2·36 — $1/2^+$

1·94 0^+
$_6C^{12} + p$

0·00 — $1/2^-$
$_7N^{13}$

proposed transition	proton energy (c.m.)	(lab.)	observed energy	target
(1)	4·97	4·59	4·50	Air
(2)	4·44	4·10	3·97	(4·5 N : 1 O)

FIG. 12. Proposed decay scheme from O^{13} and a comparison of predicted and observed energies. The dashed lines indicate transitions not ruled out by energy or known spin-parity considerations but not leading to observed proton lines.

levels of O^{15} is not known, one cannot predict the spectrum of this source. However, the important point is that all of the spectrum from a F target can be explained in a way analogous to the explanations of all the other observed spectra. One line from the air target is at the same energy as a possible line in N^{11} decay, but the excited state involed lies at 14 Mev energy so the beta decay to it would be extraordinarily highly inhibited. In any case this can only account for part of the observed spectrum from air. One of the lines from the Mg target can be accounted for by the only expected line from the decay of Na^{19}. Again this cannot account for the whole spectrum. It does not seem likely, on energetic grounds, that the other nuclides neighboring the $(2k+2, 2k-1)$ nuclides in question emit any delayed protons observable in this experiment.

The information for the construction of Figs. 10, 11, and 12 and for the various associated arguments was taken from Ajzenberg-Selove and Lauritsen (1959), Endt and van der Leun (1962), and Everling *et al.* (1961).

The hypothesis that the decay of the nuclide $(2k+2, 2k-1)$ will dominate the delayed proton spectrum from targets of both element $(2k+2)$ and element $(2k+1)$ seems to be verified. In particular, by following very reasonable rules for predicting proton lines, all the observed lines are accounted for and all those predictions based on known level properties are borne out. The existence of Mg^{21}, Ne^{17}, and O^{13} is assumed since it seems fairly certain that proton lines in the decay of each have been observed.

Observed Cross Sections

The cross sections shown in Table I are all of the order of 10 microbarns, except for the air target. The magnitudes of these cross sections support the assignments already made, in the following way. At our bombarding energies, one would expect $(p, 3n)$ and $(p, p3n)$ cross sections to be of the order of 10 millibarns. For concreteness, consider the case of Si^{25}. The estimated $Q_\beta{}^+$ is 10.3 Mev to the ground state of Al^{25}, and 3.6 Mev to the 6.70-Mev state. The corresponding end-point energies are 9.3 and 2.6 Mev respectively. On a fifth-power variation of β-transition probability, the transition to the upper state will be 1.7×10^{-3} as intense as that to the ground state. Since other transitions are also competing, we may guess roughly that the overall branching ratio to the 6.70-Mev state is around 10^{-3}. Thus the anticipated cross section for delayed protons from this level is around 10 microbarns, as observed. The other cases are similar, except for the air target where extra forbiddenness leads to lower cross sections.

SUMMARY

It has been shown that delayed proton energy groups are emitted from an aluminum target following bombardment with 97-Mev protons. The delay is due to the 0.3-sec half-life of the previously unreported nuclide Si^{25} which β^+ decays to proton-unstable excited states of Al^{25}. In the energy range from 2 to 5 Mev the dominant proton lines in all the spectra obtained were ascribed to the decay of $(2k+2, 2k-1)$ nuclides. Thus protons following β^+ decay of O^{13}, Ne^{17}, Mg^{21}, and Si^{25} were found following bombardment of the element of each nuclide as well as the element of one-lower atomic number. One would expect this pattern to continue up to calcium. Thus one expects S^{29}, Ar^{33}, and Ca^{37} to be observable via delayed proton emission.

The material presented here does little more than demonstrate the existence of delayed proton radioactivity. It seems obvious that with greater beam intensity and better energy resolution, both easily obtainable, it will be possible to observe indirectly the ground-state β^+ decay of many new proton-rich nuclides. New information about proton-emitting excited states of the nuclides involved should also be forthcoming. It would be particularly interesting to observe the delayed proton spectra at lower energies than was attempted here (below 2.5 Mev). One would expect proton lines at these energies to be more intense and perhaps more numerous.

ACKNOWLEDGMENTS

NOTE ADDED IN PROOF: When this article was in press, we received the translation UCRL-TRANS-919 (1963) of an unpublished report JINR (Dubna) P-1072 (1962) by V. A. Karnaukhov, G. N. Ter-Akopyan, and V. G. Subbotin.

These workers searched for particles emitted from a foil acting as a catcher for products recoiling from thin targets bombarded with 130-Mev Ne^{20} ions. The detectors were E and dE/dx gas counters. With targets of both nickel and tantalum, they observed a few events due to particles with energies between 3 and 4.5 Mev, delayed by at least 0.1 sec, and much less ionizing than α particles. The authors attribute their results to delayed protons; no further information is given in their report.

REFERENCES

AJZENBERG-SELOVE, F. and LAURITZEN, T.   1959.   Nucl. Phys. **11**, 1.
BARTON, R.   1963.   Ph.D. Thesis, McGill University, Montreal.
BARTON, R. and McPHERSON, R.   1963a.   Bull. Am. Phys. Soc., Ser. II, **8**, 357.
————   1963b.   Phys. in Can. **19**, No. 3, 37.
BOOTH, E. T., DUNNING, J. R., and SLACK, F. G.   1939.   Phys. Rev. **55**, 876.
ENDT, P. M. and VAN DER LEUN, C.   1962.   Nucl. Phys. **34**, 1.
EVERLING, F., KOENIG, L. A., MATTAUCH, J. H. E., and WAPSTRA, A. H.   1961.   1960 Nucl.
      Data Tables, U.S. At. Energy Comm.
GOLDANSKY, V. I.   1960.   Nucl. Phys. **19**, 482.
————   1961.   Nucl. Phys. **27**, 648.
LE COUTEUR, K. J.   1955.   Proc. Roy. Soc. (London), Ser. A, **232**, 236.
McPHERSON, R. and BARTON, R.   1963.   Phys. in Can. **19**, No. 3, 36.
MOORE, R. B.   1962.   Ph.D. Thesis, McGill University, Montreal.
MOTTELSON, B. and NILSSON, S. G.   1959.   Kgl. Danske Videnskab. Selskab, Mat. Fys.
      Skrifter, **1**, No. 8.
PAPPAS, A. C. and RUDSTAM, G.   1960.   Nucl. Phys. **21**, 353.
ROBERTS, R., MEYER, R. D., and WANG, P.   1939.   Phys. Rev. **55**, 876.
SEEGER, P. A.   1961.   Nucl. Phys. **25**, 1.